PCCP

ROYAL SOCIETY OF CHEMISTRY

PAPER

View Article Online
View Journal | View Issue

Cite this: *Phys. Chem. Chem. Phys.*, 2021, **23**, 3739

Understanding Fermi resonances in the complex vibrational spectra of the methyl groups in methylamines†

Qian-Rui Huang,[a] Tomoya Endo,[b] Saurabh Mishra,[c] Bingbing Zhang,[d] Li-Wei Chen,[a] Asuka Fujii,[b] Ling Jiang,*[d] G. Naresh Patwari,*[c] Yoshiyuki Matsuda*[b] and Jer-Lai Kuo*[a]

Received 4th November 2020,
Accepted 25th January 2021

DOI: 10.1039/d0cp05745b

rsc.li/pccp

Vibrational spectra of the methyl groups in mono-methylamine (MMA), dimethylamine (DMA), and trimethylamine (TMA) monomers and their clusters were measured in three experimental set-ups to capture their complex spectral features as a result of bend/umbrella-stretch Fermi resonance (FR). Multiple bands were observed between 2800 and 3000 cm^{-1} corresponding to the methyl groups for MMA and DMA. On the other hand, the corresponding spectrum of TMA is relatively simple, exhibiting only four prominent bands in the same frequency window, even though TMA has a larger number of methyl groups. The discrete variable representation (DVR) based *ab initio* anharmonic algorithm with potential energy surface (PES) at CCSD/aug-cc-pVDZ quality is able to capture all the experimentally observed spectral features across all three amines, and the constructed vibrational Hamiltonian was used to analyze the couplings that give rise to the observed FR patterns. It was observed that the vibrational coupling among CH stretch modes on different methyl groups is weak (less than 2 cm^{-1}) and stronger vibrational coupling is found to localize within a methyl group. In MMA and DMA, the complex feature between 2850 and 2950 cm^{-1} is a consequence of closely packed overtone states that gain intensities by mixing with the stretching modes. The simplification of the spectral pattern of TMA can be understood by the red-shift of the symmetric CH_3 stretching modes by about 80 cm^{-1} relative to MMA, which causes the symmetric CH_3 stretch to shift outside the FR window.

Introduction

The importance of amines in chemistry, biology, and atmospheric sciences cannot be overstated. Vibrational spectroscopic measurements and their assignments aid insights into the intermolecular interactions of amine functional groups in various biomolecules.[1] In atmospheric sciences, new particle formation (NPF) is driven by aggregation of sulfuric acid and ammonia along with significant contributions from alkylamines. The presence of various amines in NPF is correlated with enhanced growth kinetics,[2] thus finding efficient ways to differentiate alkylamines is desired. In organic chemistry, the identification of primary and secondary amines *via* vibrational spectroscopy relies mostly on the NH stretching modes. However, in the clusters and condensed phases, the NH stretching modes are often broadened due to hydrogen-bonding, which is further affected by bend-stretch Fermi resonances (FR).[3] On the other hand, the vibrational spectroscopic features of the alkyl-groups of amines are much sharper, and can in principle be more suitable for the identification of amines. Additionally, in the case of tertiary amines, in the absence of an NH group, the vibrational spectroscopic identification is limited to the alkyl groups. However, the vibrational spectral features of methyl groups are often complex due to the FR coupling between C–H stretching fundamental and bending overtone states. Therefore, it is imperative to understand the vibrational spectral features of methyl groups in methylamines. The simplest of primary, secondary and tertiary amines, *viz.*, methylamine (MMA), dimethylamine (DMA), and trimethylamine (TMA), respectively, were recently investigated using the infrared-vacuum ultraviolet (IR-VUV) double resonance spectroscopic method.[3–8] The vibrational spectrum of neutral MMA dimer in the 2800–3000 cm^{-1} region shows complex features associated with the C–H stretching vibrations of the methyl group.[4]

[a] *Institute of Atomic and Molecular Sciences, Academia Sinica, Taipei 10617, Taiwan. E-mail: jlkuo@pub.iams.sinica.edu.tw*
[b] *Department of Chemistry, Graduate School of Science, Tohoku University, Aramaki-Aza-Aoba 6-3, Aoba-ku, Sendai, 980-8578, Japan. E-mail: yoshiyuki.matsuda.d4@tohoku.ac.jp*
[c] *Department of Chemistry, Indian Institute of Technology Bombay, Powai, Mumbai 400076, India. E-mail: naresh@chem.iitb.ac.in*
[d] *State Key Laboratory of Molecular Reaction Dynamics, Collaborative Innovation Center of Chemistry for Energy and Materials (iChEM), Dalian Institute of Chemical Physics, Chinese Academy of Sciences, Dalian 116023, China. E-mail: ljiang@dicp.ac.cn*

† Electronic supplementary information (ESI) available. See DOI: 10.1039/d0cp05745b

Furthermore, the vibrational spectra of neutral DMA clusters (from dimer to pentamer) in the C–H stretching region show well-resolved features, with marginal dependence on the cluster size.[5] On the other hand, the spectra of neutral and cationic TMA monomer and its clusters, in contrast to the clusters of MMA and DMA, interestingly show a much simpler vibrational spectral pattern with the presence of only four prominent bands.[6–9] The simplified spectral pattern of TMA relative to MMA and DMA is counter-intuitive since TMA has a larger number of methyl groups, and the vibrational coupling between various methyl groups in TMA is expected to complicate the FR pattern.

Several attempts have been documented in the literature to understand the complex spectral feature as a result of FR coupling. Theoretical analysis of FR observed in the alkyl C–H stretching region of hydrocarbons by Sibert and co-workers involved construction of a model Hamiltonian with rescaled stretch fundamental and bending overtones to fit the experimental data.[10–14] Alternative computational treatment on the FR of methyl-groups on amines has been attempted by Kuo and coworkers using an *ab initio* approach based on quartic potential generated at the MP2/aug-cc-pVDZ level and the corresponding eigenvalue problem was solved by the vibrational configurational interaction (VCI) method.[5,15] It was pointed out that a higher level of electronic structure theories (beyond MP2/aug-cc-pVDZ) as well as high-order terms of potential energy surface (PES), beyond quartic potential, are required to accurately capture the intensity borrowing in the FR pattern of the methyl group on the DMA clusters.[5] It is known that the FR pattern is sensitive to the efficiency of the intensity distribution, and thus reliable assessments on the relative intensities of the observed peaks from experimental spectra would be very critical to benchmark the accuracy of computational schemes. On the theoretical side, an accurate estimate of the peak positions of both the fundamental of the stretch modes and overtones states of umbrella/bending modes and their coupling strength to stretching fundamentals is essential for the analysis. In this work, investigations on the vibrational spectra of the methyl groups of MMA, DMA, and TMA monomers and clusters were carried out as a combined effort to compare experimental spectra sourced from the three different research groups at Dilan Institute of Chemical Physics (DICP), Tohoku University (TU) and Indian Institute of Technology Bombay (IITB). *Ab initio* anharmonic algorithms with PES and dipole moment surface (DMS) up to CCSD/aug-cc-pVDZ were used to analyze the vibrational coupling and FR patterns of the methyl groups in these three amines. Comparison between experimental data and high-level *ab initio* calculations (for both electronic and nuclear degrees of freedom) enabled the analysis of the FR pattern in the three amines. Additionally, the vibrational coupling among different functional groups was also explored.

Methodology

(A) Experimental

Three experimental set-ups from DICP, TU, and IITB were employed to record the vibrational spectra of MMA, DMA, and TMA neutral monomers and their homo-clusters and are summarized below.

Details of the Dalian IR-VUV double resonance spectroscopy apparatus have been described previously.[4] Briefly, neutral clusters were generated by supersonic expansions of an MMA-argon (or DMA-helium, TMA-helium) mixture using a pulsed valve (General Valve, Series 9). For the IR excitation of the clusters, we used a tunable IR optical parametric oscillator/amplifier system (LaserVision). Subsequent photoionization was carried out with about 50 ns delay with 118 nm VUV light generated by third-harmonic generation (355 nm) of an Nd:YAG laser (Nimma-600) *via* a Xe/Ar gas mixture at 1 : 10 relative concentration for 200 Torr total pressure. The VUV laser was operated at 20 Hz and the IR laser was operated at 10 Hz. IR spectra were recorded in the difference modes of operation (IR laser on-IR laser off).

In the TU setup for the IR spectroscopy of the MMA, DMA, and TMA monomers, each sample diluted by the He carrier gas was supersonically expanded into a vacuum chamber. The jet-cooled sample was ionized by 118 nm VUV light and all produced ions were mass-analyzed and detected by the time-of-flight mass spectrometer. The IR spectrum of each neutral monomer was observed by IR-VUV double resonance spectroscopy.[16] The IR light was introduced 20 ns prior to the 118 nm photoionization, and the H-loss fragment ion produced by the IR absorption followed by the VUV photoionization was detected. By scanning the IR frequency while monitoring the fragment yield, an IR spectrum was measured. The IR light was generated by different frequency mixing between the second harmonic of an Nd:YAG laser (Powerlite 8010, Continuum) and a dye laser output (ND-6000, Continuum) operated with the DCM dye, by the use of a $LiNbO_3$ crystal.

The experimental setup for carrying out experiments in IIT-Bombay is described elsewhere.[17] Briefly, 50% aqueous methylamine seeded in helium gas at 2 atm pressure was expanded to form a free-jet using a 0.5 mm orifice nozzle pulsed valve (Series-9, Iota one; General valve) into a vacuum chamber. A two-stage Wiley-McLaren time-of-flight mass spectrometer attached with a channel electron multiplier (CEM-KBL-25RS; Sjuts Optotechnik) and a preamplifier (SR445A; Stanford Research Systems) was used to observe the mass signal of the MMA dimer and trimer. The IR spectra in the CH stretching region were recorded using the IR-UV double resonance spectroscopic method.[18,19] The MMA dimer and trimer were resonantly ionized with a 213 nm laser, which is the fifth harmonic of an Nd:YAG laser (TRLiG 850-10; Litron), and the vibrational excitation was achieved using a tuneable IR laser, which was an idler component of a $LiNbO_3$ OPO (Custom IR OPO; Euroscan Instruments), pumped by an injection-seeded Nd:YAG laser (Brilliant-B; Quantel).

(B) Computational

Low-energy conformers of the clusters of the three amines were searched using a random sampling method in combination with density functional theory[4,5,15] and the resulting distinct geometries were optimized using the MP2/aug-cc-pVDZ level (see the ESI†). The structures of the low-energy conformers are shown in Fig. 1 and their Cartesian coordinates can be found in Table S1 (see the ESI†). For MMA and DMA, there are two

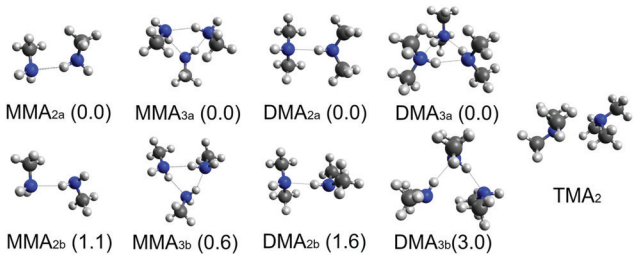

Fig. 1 Structure of low-energy conformers of the dimers and the trimers of MMA and DMA and the dimer of TMA optimized at the MP2/aug-cc-pVDZ level. The relative stabilization energies (kcal mol^{-1}) are shown in parentheses.

distinct low-energy hydrogen-bonded conformers with an energy difference of about 1 kcal mol^{-1}. The structure of the global minimum of the TMA dimer is not hydrogen-bonded; however, a few other conformers with relative energy higher than 1 kcal mol^{-1} were found, but are not included in this work. All electronic structure calculations were carried out using the Gaussian 16 package.[20]

The *ab initio* anharmonic calculations included six localized normal modes (LNMs): three C–H stretching, two bending, and one umbrella mode on a single methyl group in each molecule and each molecular cluster (shown in Table S2 in the ESI†). To obtain the LNM, we firstly obtain the analytical hessian matrix at the level of MP2/aug-cc-pVDZ; after that, we perform the partial hessian vibration analysis (PHVA)[21,22] to obtain the LNM on a single methyl group. For a better accuracy than quartic potential, the *ab initio* anharmonic algorithms discrete variable representation (DVR)[23,24] approach in which the PES and DMS are expressed on a direct product of Gauss-Hermite quadrature along the selected vibrational normal modes with high-level electronic structure methods was used. In an earlier work on the vibrational spectra of the methyl-groups of MMA and DMA,[5,15] it was shown that five grid points are adequate along all the modes, *viz.*, stretching fundamentals and overtones of umbrella and bending for calculating the spectra. Furthermore, in the literature, it has been suggested that the origin of the intensity of the overtone bands can be sensitive to the choice of coordinate systems. In the case of CO_2, however, Sibert *et al.* have shown that the FR coupling strength is almost identical in rectilinear and curvilinear coordinates[25] and even with coordinates of arbitrary curvature.[26] Therefore, due to the simplicity of the kinetic energy operator, the vibrational Hamiltonian is expressed in rectilinear coordinates in the present work.

To simplify the discussion on FR of the methyl group of the three amines considered in the present work, the naming scheme used for MMA to describe the normal modes is as follows. The six 6 degrees of freedom (DoF) utilized are $CH_3^{a''}$d-str (ν_{11}), $CH_3^{a'}$d-str (ν_2), $CH_3^{a'}$s-str (ν_3), $CH_3^{a''}$d-deform (ν_{12}), $CH_3^{a'}$d-deform (ν_5), and $CH_3^{a'}$s-deform (ν_6).[27] The PES can be expanded using the *n*-mode representation (*n*MR) scheme proposed by Bowman,[28]

$$V(q_i, q_j, q_k, \ldots) = V^{(0)} + \sum_i \Delta V^{(1)}(q_i) + \sum_{ij} \Delta V^{(2)}(q_i, q_j) + \sum_{ijk} \Delta V^{(3)}(q_i, q_j, q_k) + \cdots$$

where $V^{(0)}$ is the potential energy at the equilibrium point, $\Delta V^{(1)}$ is the change in energy within a single normal mode q_i, $\Delta V^{(2)}$ is the coupling between two modes q_i and q_j, and so on. Based on this nMR approximation, we can engage more than one electronic structure method to construct the PES.[29] To balance the computational accuracy and efficiency, we chose the following settings: $V^{(0)}$ to $\Delta V^{(2)}$ terms are most essential and thus were calculated with the CCSD/aug-cc-pVDZ level to improve the accuracy of the peak position. $\Delta V^{(3)}$ and $\Delta V^{(4)}$ terms were evaluated at the MP2/aug-cc-pVDZ level and $\Delta V^{(5)}$ and $\Delta V^{(6)}$ terms were neglected. The multi-dimensional Hamiltonian under DVR representation can be directly diagonalized using ARPACK[30] in SciPy[31] packages. The absorption intensities of vibrational transitions are evaluated based on the Fermi golden rule from the eigenvectors and the DMS.

Results and discussion

The IR spectra of the MMA monomer, dimer, and trimer in the C–H stretching regions are shown in Fig. 2. The spectrum of the MMA monomer (Fig. 2a; measured at TU) shows four distinct bands centred around 2965, 2908, 2885 and 2818 cm^{-1}. The spectrum of the MMA dimer (Fig. 2b; measured at DICP)[4] shows that the three high-frequency bands observed in the monomer (Fig. 2a) are split into six bands at 2878, 2897, 2912, 2928, 2954, and 2975 cm^{-1}. Furthermore, a weak band round 2800 cm^{-1} can be seen in the MMA dimer, only when the IR laser power exceeds 10 mJ mm^{-2}. This band has been assigned to be the overtone of an umbrella mode[15] and its existence is

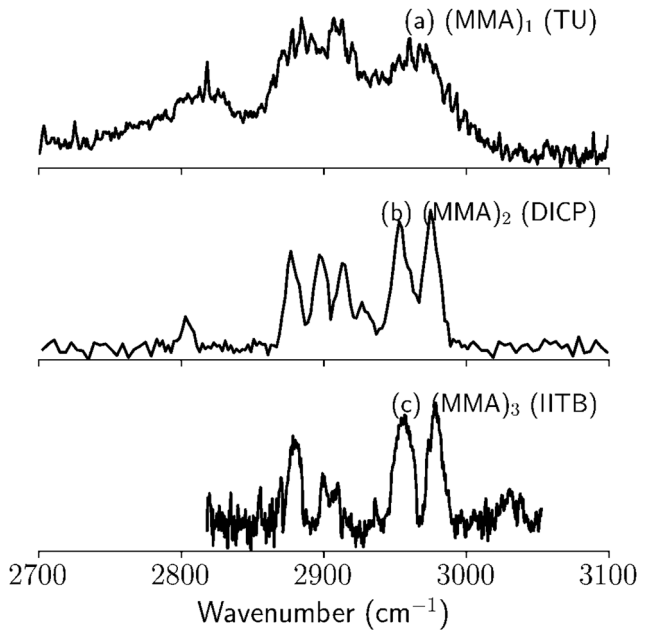

Fig. 2 IR spectra of MMA (a) monomer [TU], (b) dimer [DICP] and (c) trimer [IITB] in the C–H stretching region. The difference between (b) and (c) at ~2900 cm^{-1} is not caused by the size of the cluster; it is due to the different experimental setups in different groups (see Fig. S1, ESI†).

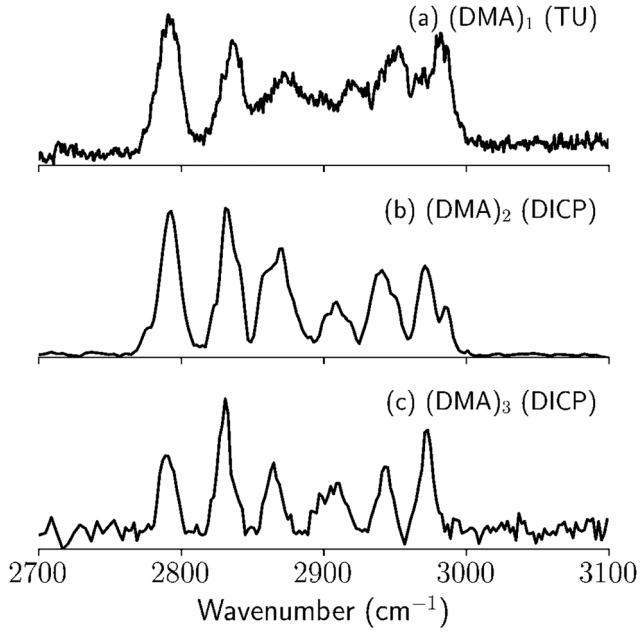

Fig. 3 IR spectra of MMA (a) monomer [TU], (b) dimer [DICP], and (c) trimer [DICP] in the C–H stretching region.

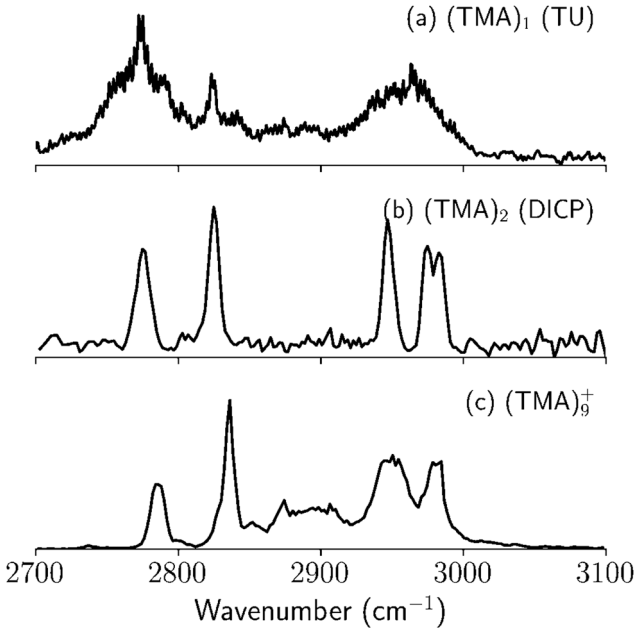

Fig. 4 The IR spectra of TMA (a) monomer [TU] and (b) dimer [DICP] in the C–H stretching region. The IR spectrum of the (c) TMA nonamer cation [DICP][9] is included for the sake of comparison.

confirmed by the spectrum of the MMA monomer (Fig. 2a). The spectrum of the MMA trimer (Fig. 2a; measured at IITB) is very similar to the dimer (see Fig. S1 (ESI†) for comparison of the MMA dimer spectrum recorded at DICP and IITB). The marginal differences in the spectra of the dimer (2b) and the trimer (2c) and those in Fig. S1 (ESI†) can be attributed to the differences in the experimental methodologies and lack of laser-power normalization. The vibrational pattern is consistent from monomer to trimer and appears to be originating from the methyl group of the MMA which indicates that the observed spectral features are unique to the methyl group of MMA and are limited by the intramolecular couplings.

Fig. 3 depicts the spectra of the DMA monomer, dimer, and trimer in the C–H stretching region. The spectrum of the DMA monomer (Fig. 3A; measured at TU) shows six (almost) evenly spaced bands between 2790 and 2970 cm^{-1}. The corresponding spectra of the dimer and trimer (Fig. 3b and c; recorded at DICP) differ marginally relative to the monomer.[5] However, the band around 2950 cm^{-1} could only be observed under higher laser fluence (around 7.2 mJ mm^{-2}). Furthermore, the band around 2900 cm^{-1} shows splitting in the DMA trimer. It is noteworthy that the spectra of the DMA clusters from dimer to pentamer were measured by the DICP team, with very marginal size-dependence of the spectra of the methyl groups.[5] The vibrational spectral features of the methyl groups in DMA are more complicated than those in MMA. Since DMA has two methyl groups, it is intuitive to expect additional complexity arising out of coupling between the two methyl groups in DMA.

The IR spectrum of the TMA monomer (Fig. 4a; recorded at TU) shows three prominent bands, while the corresponding spectrum of the TMA dimer (Fig. 4b; recorded at DICP) shows four bands centered around 2975, 2949, 2823, and 2770 cm^{-1}.[8] Comparison of the spectra of the TMA monomer and the dimer indicates splitting of the high-frequency band at 2975 cm^{-1}. Additionally, it has been reported that a low-frequency band appears at 2740 cm^{-1} only under higher laser power conditions ($\sim$4.5 mJ mm^{-2}).[8] In the IR spectrum of the TMA monomer, we find the correspondence to all the bands in the spectrum of the dimer, and the band at 2740 cm^{-1} is not obvious/visible under the present condition. Further, the spectra of the TMA cluster cations [$(TMA_n)^+$ n = 3–9; measured at DICP] show features that are almost identical to the TMA dimer.[9] These results suggest that the TMA dimer adequately represents the IR spectral features of the TMA neutral and cationic clusters.

Comparison of the experimental spectra of the methyl group in the amine monomers and clusters suggests that the spectral features in the C–H stretching region are sensitive to the degree of substitution on the amine nitrogen (primary *vs.* secondary *vs.* tertiary), rather than the size of the cluster. However, the present set of experimental spectra clearly indicates that the spectral features of DMA are more complex than those of MMA, while the spectra of TMA and its clusters are the simplest. In general, the FR is likely to play an important role. Herein, it is demonstrated that the *ab initio* anharmonic algorithms with PES and DMS evaluated at the CCSD/aug-cc-pVDZ level of electronic structure can faithfully capture the details of the experimentally observed spectra. Furthermore, the calculated spectra will allow the elucidation of the zero-order vibrational states and the consequent FR couplings. In the earlier theoretical studies, it has been found that vibrational coupling is localized on a single methyl group involving three fundamental normal modes and three overtones (a total of six modes). Additionally, in MMA the coupling between the modes of the methyl and amino

groups was found to be very weak as evident from the almost identical spectral features simulated with or without explicitly including the cross-coupling between the two sets of modes. This notion of localization of vibrational coupling is consistent with the fact that the stretching modes tend to localize on functional groups.[32,33] Recent studies on the analysis of the FR coupling in the NH stretching vibrations of ammonia[34] and methylamine,[3] indicate that the usage of the normal modes localized on a specific functional group captures the main spectral features and leads to quick convergence. To further confirm weak coupling between the vibrations of two methyl groups, vibrational spectra of a single methyl group (6D) and two groups (12D) were simulated and the comparison is shown in Fig. S2 (see the ESI†), which indicates that the coupling between two methyl groups leads to minor splitting and broadening of some bands.

The IR absorption spectra of the methyl groups of MMA, DMA, and TMA monomers simulated with the above-mentioned *ab initio* anharmonic algorithms are shown as blue traces in Fig. 5. The peak positions and relative intensities compare well with the corresponding experimental spectra depicted in Fig. 2–4. The experimental spectra are also shown in Fig. 5 as grey traces for the sake of direct comparison. The agreement between the simulated and experimental spectra is not only a strong confirmation of the accuracy of the *ab initio* anharmonic algorithms and the quality of PES constructed at the CCSD/aug-cc-pVDZ level but also the localization of vibrational coupling that leads to the FR pattern. Therefore, it is worthwhile to carry out a more detailed analysis of the vibrational Hamilton in order to decode the coupling that leads to the change in the FR patterns.

To check the difference between the spectra of the methyl groups on the monomer and those in the cluster, simulations were performed on the spectra of a methyl group in the trimers of MMA and DMA (MMA_{3a} and DMA_{3a}) and are also depicted in Fig. 5 (blue traces). Also shown, for the sake of comparison, are the corresponding experimental spectra (grey traces). On the whole, the spectral features of the clusters are similar to those of monomers, with some bands shifted by as much as 10–15 cm^{-1}, with marginal dependence on the cluster size. The main difference between the monomer and cluster is the broader peaks due to the wider rotational contour. For example, ν_2 and ν_{11} in the MMA and TMA monomer were merged to a single broad band, but in the MMA trimer and TMA dimer these two peaks can be resolved. It must be pointed out that the present set of simulation with the DVR method (which includes high-order terms) using the PES calculated at the CCSD/aug-cc-pVDZ level improves the peak positions of ν_3 and ν_{11} by about 40 cm^{-1}, in comparison with the earlier method wherein quartic potential was evaluated at the MP2/aug-cc-pVDZ level of theory.[5] The preliminary analysis on DMA was reported earlier,[5] and in the present work, consistent improvement in the spectral features was observed for the clusters of MMA and TMA.

In order to assist the assignment and analysis of the vibrational coupling behind the observed FR pattern of the methyl

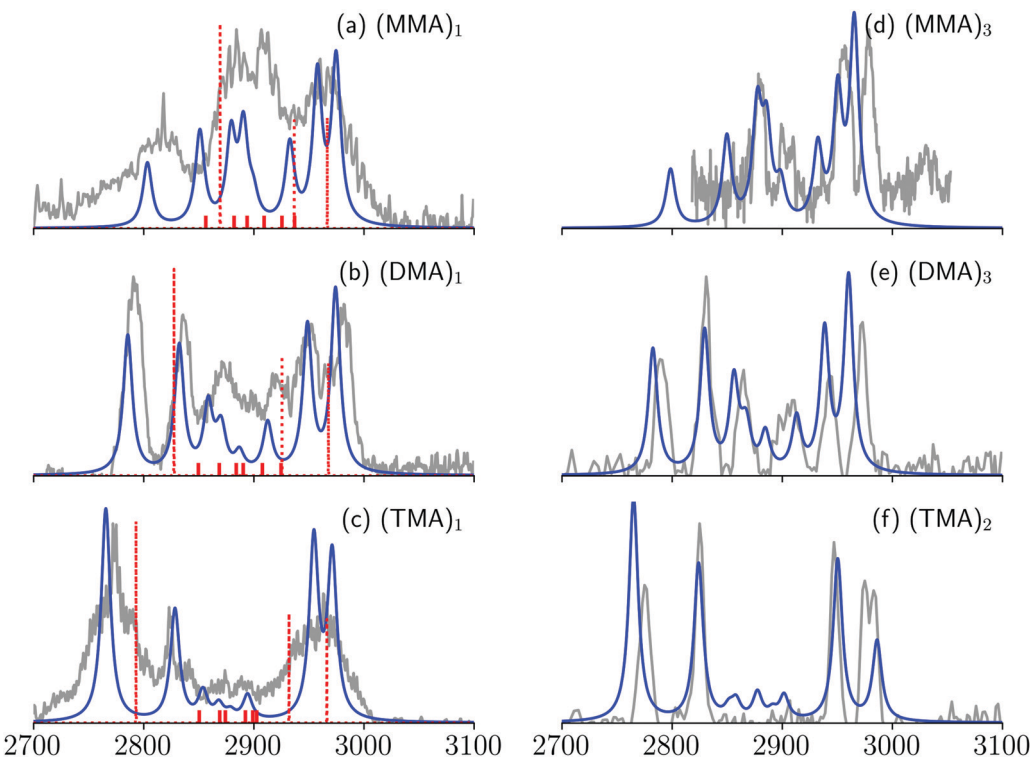

Fig. 5 Left panel: Simulated IR absorption spectra of the methyl groups of (a) MMA, (b) DMA and (c) TMA monomers simulated with *ab initio* anharmonic algorithms (blue traces). The dotted and the solid sticks indicate peak positions of three C–H stretching fundamentals and six overtone states of umbrella/bending evaluated using the FBR method (see Fig. S4 (ESI†) for a version with assignments). The experimental spectra are shown as grey traces for the sake of comparison. Right panel: Simulated IR absorption spectra (blue traces) of the methyl groups of (d) MMA-trimer, (e) DMA-trimer and (f) TMA-dimer along with their experimental spectra (grey traces).

groups, a direct product of the eigenvectors of the 3D Hamiltonian of umbrella/bending (ub) modes (ν_5, ν_6 and ν_{11}) and the 3D Hamiltonian of stretching (S) modes (ν_2, ν_3 and ν_{12}) as the basis was used to recast the 6D vibrational Hamiltonian. Such a transformation of vibrational Hamiltonian is referred to as Finite Basis Representation (FBR)[35] or Pure State (PS)[36] in the literature. A sub-matrix of the nine quantum states involved in FR under FBR of the three amines are compiled in Table S3 (see the ESI†). The diagonal terms, $\langle(ub)_0,S_1|H|(ub)_0,S_1\rangle$ and $\langle(ub)_2,S_0|H|(ub)_2,S_0\rangle$, stand for the peak positions of three C–H stretching fundamental and overtone states of umbrella/bending. Their peak positions are also shown in Fig. 5 as dotted and solid sticks, respectively, for better comparison with the simulated spectra. From the peak positions indicated in Fig. 5, it is evident that the position of asymmetric stretching (ν_2 and ν_{11}) fundamentals remain almost unaltered, however, the overtone/combination states of (ν_5, ν_6 and ν_{11}) get red-shifted progressively with an increase in the number of methyl groups from MMA to TMA. The most discernable change is the red-shift of symmetric CH_3 stretching (ν_3) by about 80 cm^{-1} from MMA to TMA (see the lowest frequency dashed line in the left panel of Fig. 5). Based on the peak positions, the two bands centered around 2950 and 2975 cm^{-1} can be assigned to ν_2 and ν_1 C–H stretching modes and it is clearly evident that the spectral features of TMA are simpler than MMA and DMA, since the ν_3 band in TMA has moved out of the resonance window.

To gain further insights into the FR coupling and to confirm the above analysis, the off-diagonal terms in Table S3 (see the ESI†) were examined for the coupling strength between two quantum states using the direct product of 3 stretching modes and 3 umbrella/bending modes. It was observed that the coupling among quantum states in the same manifold is weak (less than 3 cm^{-1}). The strongest coupling was found between $2\nu_6$ and ν_3/ν_2 with a magnitude of about 30 cm^{-1}. Due to this coupling, $2\nu_6$ borrows intensity; therefore the lowest frequency mode of MMA at 2803 cm^{-1} can be assigned to $2\nu_6$. Similarly, in DMA and TMA the $2\nu_6$ plays an important role in the two low-frequency modes. Detailed assignment of the simulated spectra can be carried out by analyzing the square of the inner product between the eigenfunctions and the FBR basis sets. Table 1 lists all the prominent peak positions along with their intensity and projection over the nine quantum states, which contribute to over 99% of the eigenfunctions. This confirms that the sub-matrices shown in Table S1 (ESI†) can be used quantitatively. The qualitative assignments on the high- and low-frequency peaks discussed in the previous paragraph can be confirmed by the analysis in Table 1. The peaks between 2850 and 2950 cm^{-1} are more complex as there are five or six quantum states packed within these 100 cm^{-1} windows with coupling strength as strong as 20 cm^{-1}. In the case of TMA, since the stretching modes are outside this FR window the intensity

Table 1 Simulated spectra of a methyl group on MMA, DMA and TMA monomer and their assignments. Frequency is in cm^{-1} and intensity in km mol^{-1}. The assignment is conducted by analyzing the square of the inner product between the eigenfunctions and the corresponding FBR basis sets

Freq.	Int. (%)	ν_3 (%)	ν_2 (%)	ν_{11} (%)	$2\nu_6$ (%)	$\nu_6+\nu_5$ (%)	$\nu_6+\nu_{12}$ (%)	$2\nu_5$ (%)	$\nu_5+\nu_{12}$ (%)	$2\nu_{12}$ (%)
MMA_1										
2803.7	18.2	27.8	4.2	0.0	63.1	0.6	0.0	2.2	0.0	1.3
2851.3	26.6	20.5	7.2	0.0	10.3	58.8	0.0	0.1	0.0	2.3
2877.4	1.1	0.0	0.0	1.8	0.0	0.0	97.0	0.0	0.6	0.0
2879.7	23.6	22.0	0.1	0.0	17.0	22.0	0.0	31.5	0.0	6.8
2890.9	26.5	12.1	14.8	0.0	0.0	16.7	0.0	50.6	0.0	5.0
2899.9	6.4	0.0	0.0	16.0	0.0	0.0	1.5	0.0	81.9	0.0
2933.0	22.4	8.7	10.4	0.0	0.0	1.1	0.0	1.0	0.0	78.4
2958.0	41.9	8.5	62.9	0.0	8.6	0.0	0.0	14.0	0.0	5.7
2975.0	46.7	0.0	0.0	81.8	0.0	0.0	0.8	0.0	17.0	0.0
DMA_1										
2785.9	39.4	48.8	2.4	0.2	42.7	1.2	0.2	2.0	0.1	1.6
2832.6	36.1	23.6	11.4	0.2	29.4	31.2	0.6	0.5	1.6	0.8
2858.8	18.6	14.1	0.1	0.4	13.1	56.1	8.9	4.3	0.2	2.2
2867.4	2.3	0.4	0.3	3.3	3.1	0.0	53.6	37.7	0.9	0.0
2870.9	11.0	4.1	6.4	0.4	0.4	9.4	32.6	44.3	1.4	0.3
2887.3	5.2	0.9	5.1	6.9	1.9	0.3	2.6	0.3	72.3	9.1
2912.9	14.0	4.2	7.9	0.7	0.1	0.7	0.0	0.4	15.3	70.3
2949.0	41.4	3.3	65.0	0.6	7.3	0.3	0.3	5.8	4.1	13.0
2974.5	51.9	0.2	1.0	86.9	1.1	0.0	0.6	4.2	3.7	2.0
TMA_1										
2765.9	60.5	71.7	0.8	0.0	23.6	0.4	0.0	0.7	0.0	2.1
2828.7	31.7	18.4	14.6	0.0	51.4	10.2	0.0	3.3	0.0	1.3
2853.8	6.5	4.3	0.0	0.0	8.9	84.0	0.0	0.9	0.0	1.1
2855.4	1.6	0.0	0.0	3.6	0.0	0.0	92.9	0.0	2.8	0.0
2868.6	4.1	0.0	7.6	0.0	7.2	3.7	0.0	80.2	0.0	0.6
2879.1	2.2	0.0	0.0	6.8	0.0	0.0	4.6	0.0	88.1	0.0
2894.6	7.1	3.7	0.9	0.0	0.1	0.2	0.0	1.2	0.0	93.5
2954.8	50.9	1.4	75.7	0.0	7.7	0.7	0.0	13.2	0.0	0.9
2971.4	46.2	0.0	0.0	89.2	0.0	0.0	1.8	0.0	8.6	0.0

borrowing effect is meager. In comparison to TMA, the spectral features of MMA and DMA are more difficult to assign.

Conclusions

In many organic molecules, vibrational spectral features in the CH stretching region are filled with fruitful structural information. In this research, the experimental vibrational spectra in the C–H stretching region of the methyl groups of MMA, DMA, and TMA monomers and their homo-clusters were measured in the three experimental set-ups. The spectra reveal the complex features as a result of bend/umbrella-stretch FR coupling. It was found that the FR pattern of the methyl group is insensitive to the size of the cluster, but shows a peculiar dependence on the progressive number of methyl groups. DVR based *ab initio* anharmonic algorithms with six degrees of freedom on a methyl group in these amines were carried out to simulate the IR spectra. Good agreement between the simulated and experimental spectra not only validates the computational algorithm but also allows evaluation of vibrational coupling, which suggests that the strong FR coupling is localized within a methyl group and coupling across methyl and amine functional groups is weak. Furthermore, the FR pattern was found to be less sensitive to the number of methyl groups on the amine (primary *vs.* secondary *vs.* tertiary) and is determined by the position of the symmetric CH stretching fundamental which red-shifts from MMA, to DMA to TMA. A consistent coupling scheme between three stretching fundamental and six bending/umbrella overtones is found in these three types of amine. Finally, a simple picture based on the coupling among nine quantum states is obtained to account for the FR pattern. Since this FR pattern is intrinsic to the methyl group, the analysis presented in this work is widely applicable to FR in various types of organic molecules, which is necessary for understanding their nuclear motion.

Conflicts of interest

There are no conflicts to declare.

Acknowledgements

QRH, LWC and JLK are supported by the Ministry of Science and Technology of Taiwan (MOST 107-2628-M-001-002-MY4, MOST 107-2923-M-001-008-MY2, MOST 109-2639-M-009-001-ASP and MOST 109-2113-M-001-040), and Academia Sinica. Computational resources were supported in part by the National Center for High Performance Computing (NCHC), Taiwan. QRH thanks Academia Sinica for the Postdoctoral Research Fellowship. YM acknowledges the Grant-in-Aid for Scientific Research (Project No. 26108504 on Innovative Area [2507]) from MEXT Japan. AF acknowledges the Grant-in-Aid for Scientific Research (Project No. 18H01931) from JSPS. GNP is supported by the Science and Engineering Research Board, Department of Science and Technology (Grant No. EMR/2016/000362). SM thanks CSIR for the research fellowship. LJ is supported by the National Natural Science Foundation of China (Grant No. 21673231, 21327901, and 21688102), the Dalian Institute of Chemical Physics (No. DICP DCLS201702), and the Strategic Priority Research Program (Grant No. XDB17000000) of the Chinese Academy of Science.

References

1 M. Meot-Ner, Intermolecular forces in organic clusters, *J. Am. Chem. Soc.*, 1992, **114**, 3312–3322.
2 S. E. Waller, Y. Yang, E. Castracane, E. E. Racow, J. J. Kreinbihl, K. A. Nickson and C. J. Johnson, The interplay between hydrogen bonding and coulombic forces in determining the structure of sulfuric acid-amine clusters, *J. Phys. Chem. Lett.*, 2018, **9**, 1216–1222.
3 S. Mishra, H.-Q. Nguyen, Q.-R. Huang, C.-K. Lin, J.-L. Kuo and G. N. Patwari, Vibrational spectroscopic signatures of hydrogen bond induced NH stretch-bend Fermi-resonance in amines. The methylamine clusters and other N–H···N hydrogen-bonded complexes, *J. Chem. Phys.*, 2020, **153**, 194301, DOI: 10.1063/5.0025778.
4 B. Zhang, X. Kong, S. Jiang, Z. Zhao, D. Yang, H. Xie, C. Hao, D. Dai, X. Yang, Z. F. Liu and L. Jiang, Infrared-vacuum ultraviolet spectroscopic and theoretical study of neutral methylamine dimer, *J. Phys. Chem. A*, 2017, **121**, 7176–7182.
5 B. Zhang, Q.-R. Huang, S. Jiang, L.-W. Chen, P.-J. Hsu, C. Wang, C. Hao, X. Kong, D. Dai, X. Yang, J.-L. Kuo and L. Jiang, Infrared spectra of neutral dimethylamine clusters: An infrared-vacuum ultraviolet spectroscopic and anharmonic vibrational calculation study, *J. Chem. Phys.*, 2019, **150**, 064317.
6 T. Endo, Y. Matsuda, S. Moriyama and A. Fujii, Infrared spectroscopic study on trimethyl amine radical cation: Correlation between proton-donating ability and structural deformation, *J. Phys. Chem. A*, 2019, **123**, 5945–5950.
7 Y. Matsuda, Y. Nakayama, N. Mikami and A. Fujii, Isomer-selective infrared spectroscopy of the cationic trimethylamine dimer to reveal its charge sharing and enhanced acidity of the methyl groups, *Phys. Chem. Chem. Phys.*, 2014, **16**, 9619–9624.
8 B. Zhang, X. Kong, S. Jiang, Z. Zhao, H. Xie, C. Hao, D. Dai, X. Yang and L. Jiang, Infrared-vacuum ultraviolet spectroscopic and theoretical study of neutral trimethylamine dimer, *Chin. J. Chem. Phys.*, 2017, **30**, 691–695.
9 X. Lei, X. Kong, Z. Zhao, B. Zhang, D. Dai, X. Yang and L. Jiang, Infrared photodissociation spectroscopy of cold cationic trimethylamine complexes, *Phys. Chem. Chem. Phys.*, 2018, **20**, 25583–25591.
10 E. G. Buchanan, J. C. Dean, T. S. Zwier and E. L. Sibert, Towards a first-principles model of Fermi resonance in the alkyl CH stretch region: Application to 1,2-diphenylethane and 2,2,2-paracyclophane, *J. Chem. Phys.*, 2013, **138**, 064308.
11 E. L. Sibert, N. M. Kidwell and T. S. Zwier, A first-principles model of fermi resonance in the alkyl CH stretch region: Application to hydronaphthalenes, indanes, and cyclohexane, *J. Phys. Chem. B*, 2014, **118**, 8236–8245.

12 E. L. Sibert, D. P. Tabor, N. M. Kidwell, J. C. Dean and T. S. Zwier, Fermi resonance effects in the vibrational spectroscopy of methyl and methoxy groups, *J. Phys. Chem. A*, 2014, **118**, 11272–11281.
13 D. P. Tabor, D. M. Hewett, S. Bocklitz, J. A. Korn, A. J. Tomaine, A. K. Ghosh, T. S. Zwier and E. L. Sibert, Anharmonic modeling of the conformation-specific IR spectra of ethyl, *n*-propyl, and *n*-butylbenzene, *J. Chem. Phys.*, 2016, **144**, 224310.
14 D. M. Hewett, S. Bocklitz, D. P. Tabor, E. L. Sibert III, M. A. Suhm and T. S. Zwier, Identifying the first folded alkylbenzene via ultraviolet, infrared, and Raman spectroscopy of pentylbenzene through decylbenzene, *Chem. Sci.*, 2017, **8**, 5305–5318.
15 Q.-R. Huang, Y.-C. Li, K.-L. Ho and J.-L. Kuo, Vibrational spectra of small methylamine clusters accessed by an *ab initio* anharmonic approach, *Phys. Chem. Chem. Phys.*, 2018, **20**, 7653–7660.
16 Y. Matsuda, N. Mikami and A. Fujii, Vibrational spectroscopy of size-selected neutral and cationic clusters combined with vacuum-ultraviolet one-photon ionization detection, *Phys. Chem. Chem. Phys.*, 2009, **11**, 1279.
17 P. C. Singh and G. N. Patwari, Infrared-optical double resonance spectroscopy: A selective and sensitive tool to investigate structures of molecular clusters in the gas phase, *Curr. Sci.*, 2008, **95**, 469–474.
18 A. Fujii, T. Sawamura, S. Tanabe, T. Ebata and N. Mikami, Infrared dissociation spectroscopy of the OH stretching vibration of phenol-rare gas van der Waals cluster ions, *Chem. Phys. Lett.*, 1994, **2614**, 0–3.
19 R. H. Page, Y. R. Shen and Y. T. Lee, Infrared–ultraviolet double resonance studies of benzene molecules in a supersonic beam, *J. Chem. Phys.*, 1988, **88**, 5362–5376.
20 M. J. Frisch, G. W. Trucks, H. B. Schlegel, G. E. Scuseria, M. A. Robb, J. R. Cheeseman, G. Scalmani, V. Barone, G. A. Petersson, H. Nakatsuji, X. Li, M. Caricato, A. V. Marenich, J. Bloino, B. G. Janesko, R. Gomperts, B. Mennucci, H. P. Hratchian, J. V. Ortiz, A. F. Izmaylov, J. L. Sonnenberg, F. Ding Williams, F. Lipparini, F. Egidi, J. Goings, B. Peng, A. Petrone, T. Henderson, D. Ranasinghe, V. G. Zakrzewski, J. Gao, N. Rega, G. Zheng, W. Liang, M. Hada, M. Ehara, K. Toyota, R. Fukuda, J. Hasegawa, M. Ishida, T. Nakajima, Y. Honda, O. Kitao, H. Nakai, T. Vreven, K. Throssell, J. A. Montgomery Jr., J. E. Peralta, F. Ogliaro, M. J. Bearpark, J. J. Heyd, E. N. Brothers, K. N. Kudin, V. N. Staroverov, T. A. Keith, R. Kobayashi, J. Normand, K. Raghavachari, A. P. Rendell, J. C. Burant, S. S. Iyengar, J. Tomasi, M. Cossi, J. M. Millam, M. Klene, C. Adamo, R. Cammi, J. W. Ochterski, R. L. Martin, K. Morokuma, O. Farkas, J. B. Foresman and D. J. Fox, *Gaussian 16, Revision C.01*, Gaussian, Inc., Wallin, 2016.
21 J. D. Head, Computation of vibrational frequencies for adsorbates on surfaces, *Int. J. Quantum Chem.*, 1997, **65**, 827–838.
22 H. Li and J. H. Jensen, Partial Hessian vibrational analysis: The localization of the molecular vibrational energy and entropy, *Theor. Chim. Acta*, 2002, **107**, 211–219.
23 J. C. Light, I. P. Hamilton and J. V. Lill, Generalized discrete variable approximation in quantum mechanics, *J. Chem. Phys.*, 1985, **82**, 1400–1409.
24 B. Shizgal, *Spectral Methods in Chemistry and Physics*, Springer Netherlands, Dordrecht, 2015.
25 E. L. Sibert, J. T. Hynes and W. P. Reinhardt, Fermi resonance from a curvilinear perspective, *J. Phys. Chem.*, 1983, **87**, 2032–2037.
26 D. T. Colbert and E. L. Sibert, Variable curvature coordinates for molecular vibrations, *J. Chem. Phys.*, 1989, **91**, 350–363.
27 T. Shimanouchi, *Tables of Molecular Vibrational Frequencies Consolidated. Volume I*, 1972.
28 S. Carter, J. M. Bowman and N. C. Handy, Extensions and tests of "multimode": a code to obtain accurate vibration/rotation energies of many-mode molecules, *Theor. Chim. Acta*, 1998, **100**, 191–198.
29 Q.-R. Huang, T. Nishigori, M. Katada, A. Fujii and J.-L. Kuo, Fermi resonance in solvated H_3O^+: A counter-intuitive trend confirmed: Via a joint experimental and theoretical investigation, *Phys. Chem. Chem. Phys.*, 2018, **20**, 13836–13844.
30 R. B. Lehoucq, D. C. Sorensen and C. Yang, *ARPACK Users' Guide*, Society for Industrial and Applied Mathematics, 1998.
31 P. Virtanen, R. Gommers, T. E. Oliphant, M. Haberland, T. Reddy, D. Cournapeau, E. Burovski, P. Peterson, W. Weckesser, J. Bright, S. J. van der Walt, M. Brett, J. Wilson, K. J. Millman, N. Mayorov, A. R. J. Nelson, E. Jones, R. Kern, E. Larson, C. J. Carey, İ. Polat, Y. Feng, E. W. Moore, J. VanderPlas, D. Laxalde, J. Perktold, R. Cimrman, I. Henriksen, E. A. Quintero, C. R. Harris, A. M. Archibald, A. H. Ribeiro, F. Pedregosa, P. vanMulbregt, A. Vijaykumar, A. PietroBardelli, A. Rothberg, A. Hilboll, A. Kloeckner, A. Scopatz, A. Lee, A. Rokem, C. N. Woods, C. Fulton, C. Masson, C. Häggström, C. Fitzgerald, D. A. Nicholson, D. R. Hagen, D. V. Pasechnik, E. Olivetti, E. Martin, E. Wieser, F. Silva, F. Lenders, F. Wilhelm, G. Young, G. A. Price, G.-L. Ingold, G. E. Allen, G. R. Lee, H. Audren, I. Probst, J. P. Dietrich, J. Silterra, J. T. Webber, J. Slavič, J. Nothman, J. Buchner, J. Kulick, J. L. Schönberger, J. V. deMiranda Cardoso, J. Reimer, J. Harrington, J. L. C. Rodríguez, J. Nunez-Iglesias, J. Kuczynski, K. Tritz, M. Thoma, M. Newville, M. Kümmerer, M. Bolingbroke, M. Tartre, M. Pak, N. J. Smith, N. Nowaczyk, N. Shebanov, O. Pavlyk, P. A. Brodtkorb, P. Lee, R. T. McGibbon, R. Feldbauer, S. Lewis, S. Tygier, S. Sievert, S. Vigna, S. Peterson, S. More, T. Pudlik, T. Oshima, T. J. Pingel, T. P. Robitaille, T. Spura, T. R. Jones, T. Cera, T. Leslie, T. Zito, T. Krauss, U. Upadhyay, Y. O. Halchenko, Y. Vázquez-Baeza and S. Contributors, SciPy 1.0: fundamental algorithms for scientific computing in Python, *Nat. Methods*, 2020, 17, 261–272.
32 K. Yagi, M. Keçeli and S. Hirata, Optimized coordinates for anharmonic vibrational structure theories, *J. Chem. Phys.*, 2012, **137**, 204118.

33 X. Cheng, J. J. Talbot and R. P. Steele, Tuning vibrational mode localization with frequency windowing, *J. Chem. Phys.*, 2016, **145**, 124112.

34 B. Zhang, S. Yang, Q.-R. Huang, S. Jiang, R. Chen, X. Yang, D. H. Zhang, Z. Zhang, J.-L. Kuo and L. Jiang, Deconstructing vibrational motions on the potential energy surfaces of hydrogen-bonded complexes, *CCS Chem.*, 2020, 829–835.

35 J. M. Bowman, T. Carrington and H.-D. Meyer, Variational quantum approaches for computing vibrational energies of polyatomic molecules, *Mol. Phys.*, 2008, **106**, 2145–2182.

36 J. A. Tan, J.-W. Li, C.-C. Chiu, H.-Y. Liao, H. T. Huynh and J.-L. Kuo, Tuning the vibrational coupling of H3O + by changing its solvation environment, *Phys. Chem. Chem. Phys.*, 2016, **18**, 30721–30732.